Supplementary Information

Muscle-Inspired, High-Bandwidth Ionic Actuators Enabled by Fibrillar Ion-Channel Engineering

So Young Kim[1,†], Jeong Sub Lim[1,†], Hanbin Choi[1], Minjeong Kim[1], Wonjun Baek[1] and Do Hwan Kim[1,2,3*]

[1]*Department of Chemical Engineering, Hanyang University, Seoul 04763, Republic of Korea*
[2]*Institute of Nano Science and Technology, Hanyang University, Seoul 04763, Republic of Korea.*
[3]*Clean-Energy Research Institute, Hanyang University, Seoul 04763, Republic of Korea.*

**Corresponding authors: Do Hwan Kim (dhkim76@hanyang.ac.kr)*
†These authors contributed equally to this work.

List of Supplementary Figures

Supplementary Figure 1. Effect of ionic liquid content on the mechanical and ionic properties of Nafion-based composite electrolytes.

Supplementary Figure 2. Spectroscopic confirmation of urethane bonding in PEG–silica particles and its incorporation into the Nafion matrix.

Supplementary Figure 3. ^{1}H NMR characterization of PEG-functionalized silica and its incorporation in Ps(30)-iEN.

Supplementary Figure 4. Schematic illustration of the stepwise fabrication process for the PEG–silica hybridized ionic electroactive Nafion (Ps-iEN) film.

Supplementary Figure 5. Mechanical property evaluation of i-EN(40) composites with varying content of unmodified silica particles.

Supplementary Figure 6. Electrochemical characterization of i-EN(40)-based composites with varying content of unmodified silica particles.

Supplementary Figure 7. Surface morphology comparison between i-EN(40) and Ps(30)-iEN films.

Supplementary Figure 8. Elemental distribution analysis of i-EN(40) and Ps(30)-iEN films via SEM–EDS mapping.

Supplementary Figure 9. Crystallinity analysis of Nafion-based ionic electrolytes using deconvoluted XRD profiles.

Supplementary Figure 10. Schematic comparison of ion conduction pathways in Nafion-based electrolytes with varying structural modifications.

Supplementary Figure 11. Frequency-dependent blocking force curves of Ps(x)-iEN actuators (x = 5, 15, 30) measured at 3 V.

Supplementary Figure 12. Displacement of Ps(x)-iEN actuators at 3 V and two representative frequencies (0.1 and 5 Hz).

Supplementary Figure 13. Frequency-dependent blocking force curves of the Ps(15)-iEN actuator at different applied voltages (2–4 V).

List of Supplementary Tables

Supplementary Table 1. Comparative summary of the mechanical, ionic conductivity, and design characteristics of representative polymer-based ionic electrolyte systems.

Supplementary Table 2. Comparative summary of representative ionic actuators based on Nafion composite electrolytes, including their composition, mechanical properties, and actuation performance.

List of Supplementary Movies

Supplementary Movie 1. Ps-iEN actuator enables multi-frequency bending motion

Supplementary Movie 2. Ps-iEN actuator enables voltage-dependent bending motion

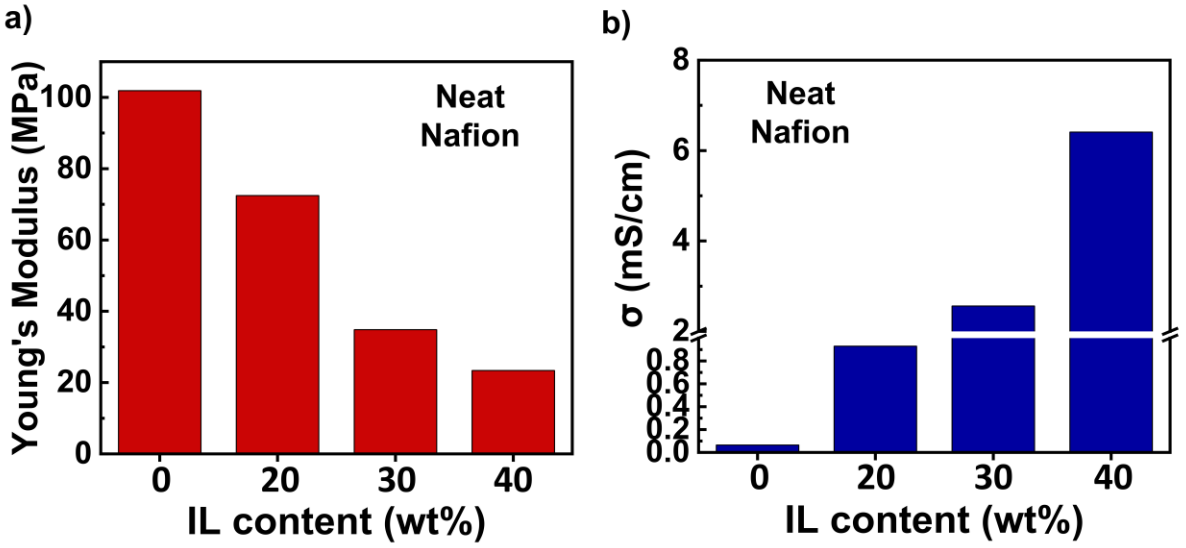

Supplementary Fig. 1. Effect of ionic liquid content on the mechanical and ionic properties of Nafion-based composite electrolytes.

(a) Young's modulus of Nafion composites with increasing IL content, showing a progressive decrease in stiffness due to the plasticizing effect of the IL. (b) Ionic conductivity of the same samples, showing steady enhancement as IL content increases, attributed to improved ionic mobility and increased free volume for transport.

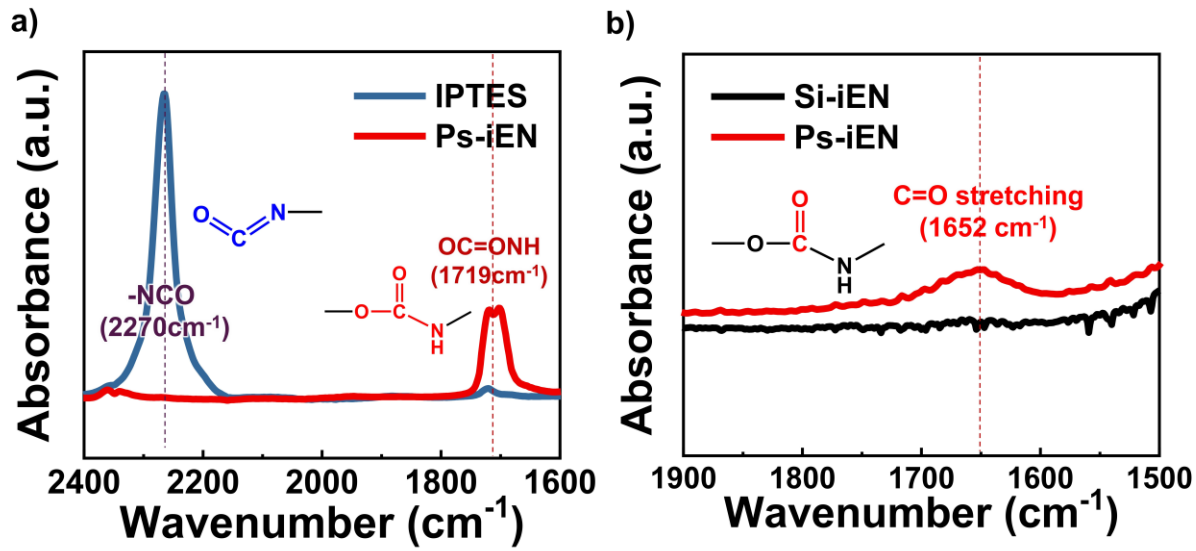

Supplementary Fig. 2. Spectroscopic confirmation of urethane bonding in PEG–silica particles and their incorporation into the Nafion matrix.

(a) FTIR spectra of PEG–NCO (blue) and PEG–silica particle (PEG–SP, red), showing the disappearance of the isocyanate peak at 2270 cm^{-1} and appearance of a urethane carbonyl peak at 1719 cm^{-1}, confirming successful bond formation. (b) FTIR spectra of Si(30)-iEN (black) and Ps(30)-iEN (red), showing a C=O stretch at 1652 cm^{-1} only in Ps(30)-iEN, indicating successful incorporation of PEG-SPs into the hybrid matrix.

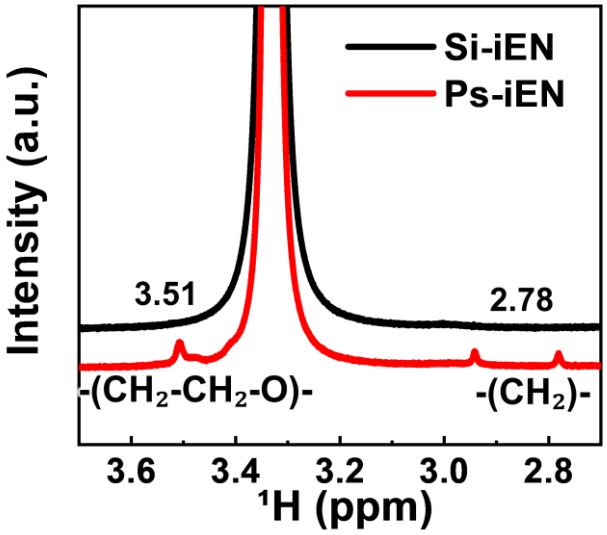

Supplementary Fig. 3. ^{1}H NMR characterization of PEG-functionalized silica and its incorporation in Ps(30)-iEN.

Comparison of ^{1}H NMR spectra of Si(30)-iEN and Ps(30)-iEN, showing PEG methylene proton signals (–CH_2–CH_2–O–) at 3.5-3.6 ppm only in Ps(30)-iEN, confirming PEG-SP integration into the Nafion matrix.

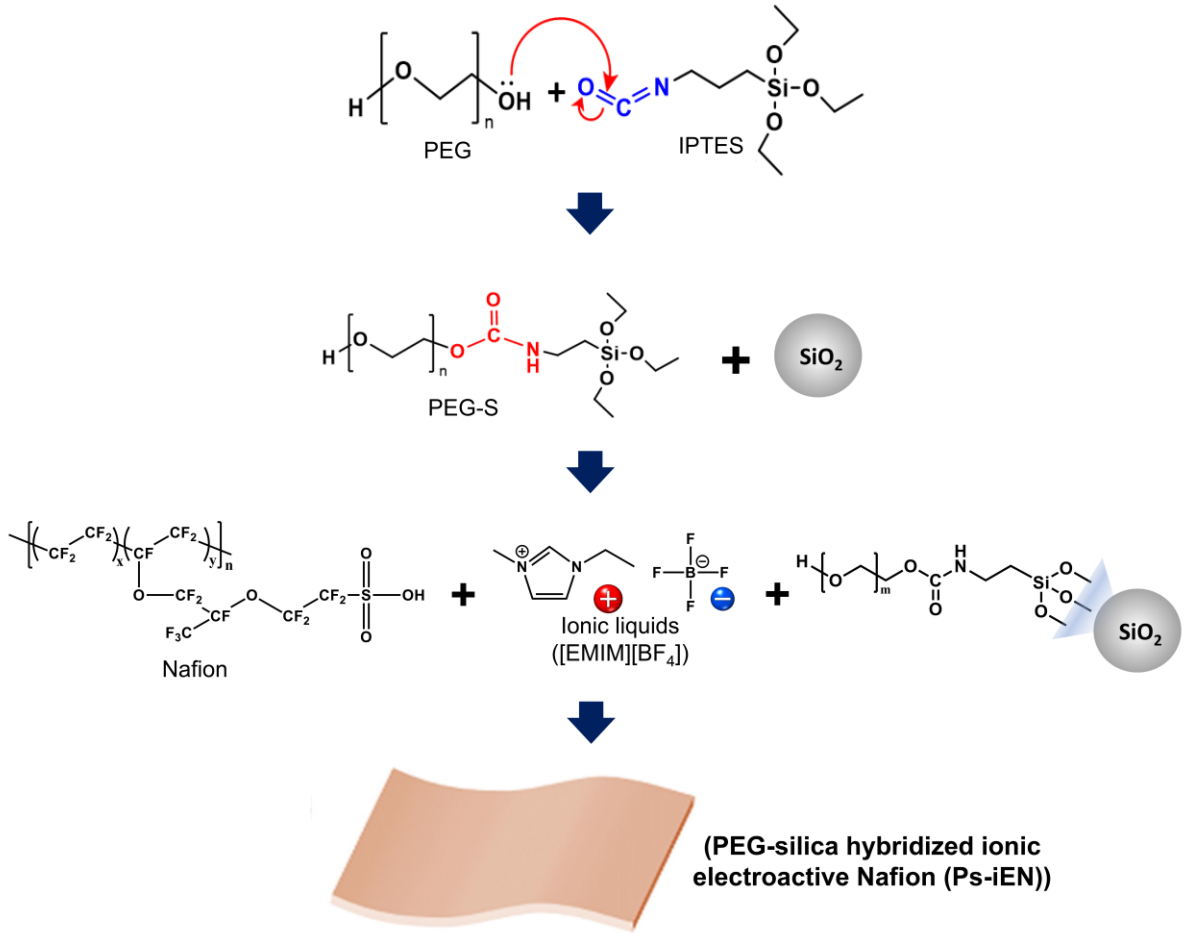

Supplementary Fig. 4. Fabrication process of the PEG–silica hybridized ionic electroactive Nafion (Ps-iEN) film.

The process involves two stages: (1) synthesis of PEG-functionalized silica particles (PEG–SPs), and (2) preparation of the Ps-iEN composite membrane. In step 1, monodisperse silica particles are reacted with 3-(triethoxysilyl)propyl isocyanate (IPTES) and PEG to form urethane bonds, followed by covalent grafting onto silica under ammonia-catalyzed conditions. In step 2, PEG-SPs and [EMIM][BF_4] are dispersed in a Nafion–DMAc solution and cast into films. Thermal treatment ensures solvent removal and uniform component integration, yielding flexible hybrid electrolytes.

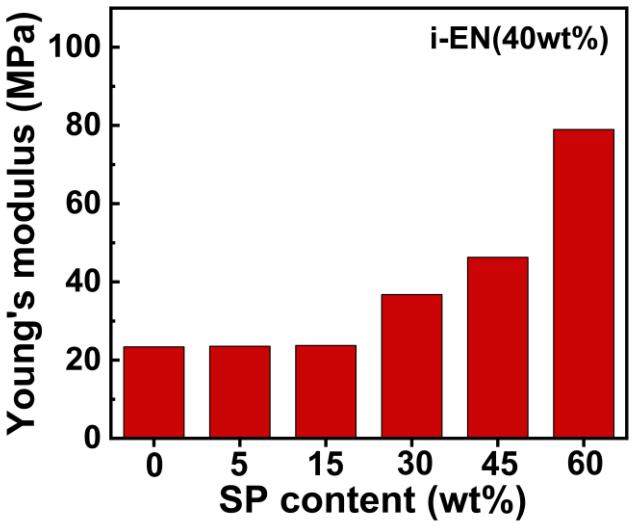

Supplementary Fig. 5. Mechanical properties of i-EN(40) composites with varying content of unmodified silica. Young's modulus of each composition, increasing monotonically with Si content due to rigid filler reinforcement.

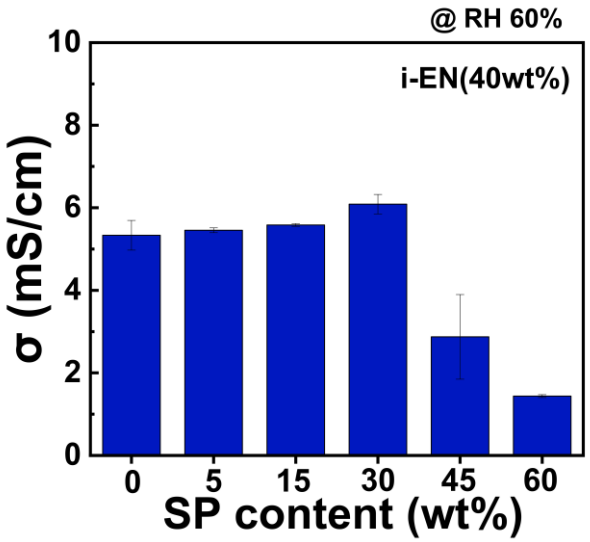

Supplementary Fig.6. Electrochemical performance of i-EN(40) composites with unmodified silica particles. Ionic conductivity with maximum conductivity at 30 wt% Si due to enhanced mobility, and decline at higher loadings from ion pathway disruption.

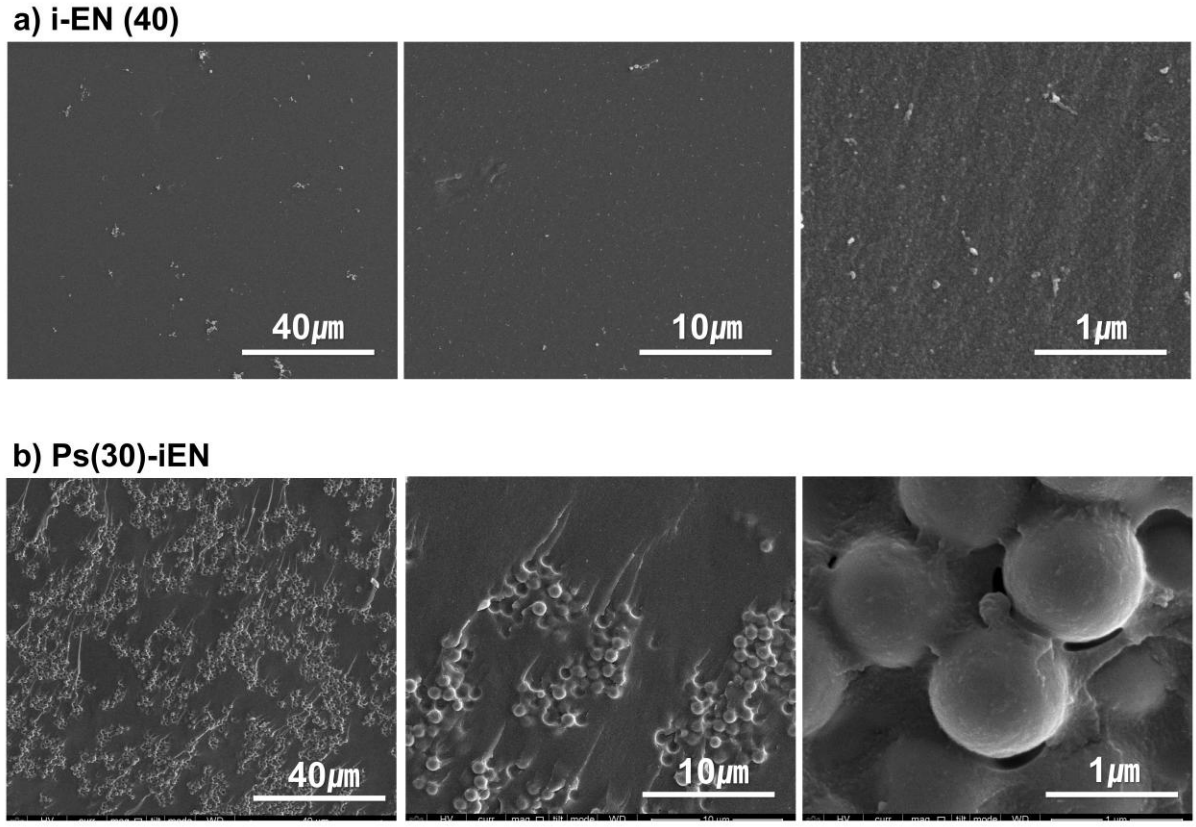

Supplementary Fig. 7. Surface morphology comparison between i-EN(40) and Ps(30)-iEN films.

(a)FE-SEM images of i-EN(40) at increasing magnifications (left to right: 40 μm, 10 μm, 1 μm) showing a smooth, featureless surface. (b) FE-SEM images of Ps(30)-iEN at the same magnifications, revealing densely dispersed PEG-SP domains within the Nafion matrix, indicating successful incorporation and interfacial compatibility.

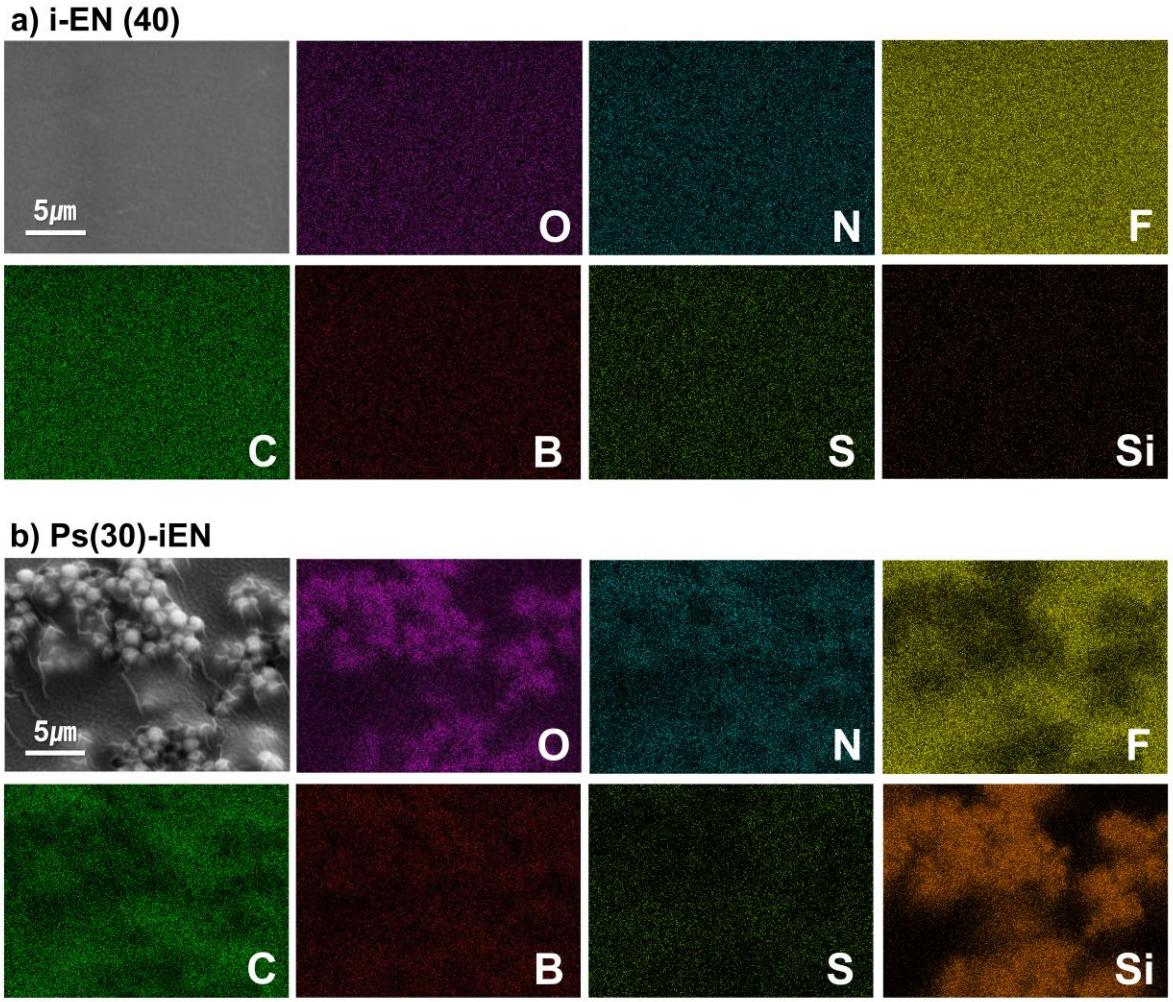

Supplementary Fig. 8. Elemental mapping of i-EN(40) and Ps(30)-iEN films via SEM–EDS.

(a) i-EN(40) shows uniform distribution of C, B, N, O, F, and S, without detectable silicon signal, indicating absence of silica fillers.(b) Ps(30)-iEN exhibits strong, localized Si signals, confirming successful incorporation of PEG-functionalized silica particles.

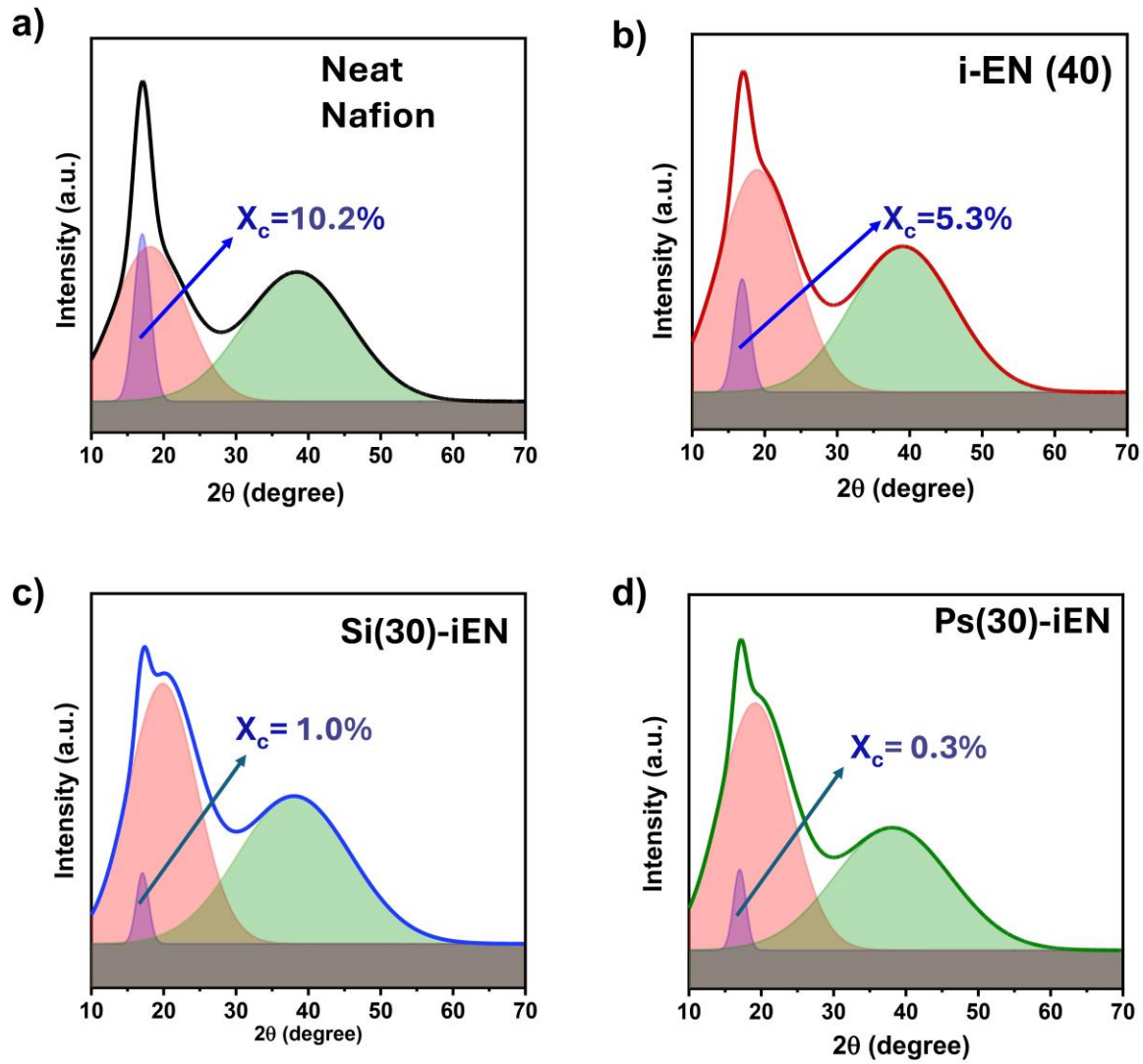

Supplementary Fig. 9. Crystallinity analysis of Nafion-based ionic electrolytes using deconvoluted XRD profiles.

(a–d) Peak fitting results for (a) Neat Nafion, (b) i-EN(40), (c) Si(30)-iEN, and (d) Ps(30)-iEN. Each XRD profile is deconvoluted into Gaussian components corresponding to amorphous and crystalline phases. The crystallinity decreases progressively with the incorporation of ionic liquid and PEG-functionalized silica, supporting structural disruption and enhanced ionic mobility in hybrid electrolyte systems.

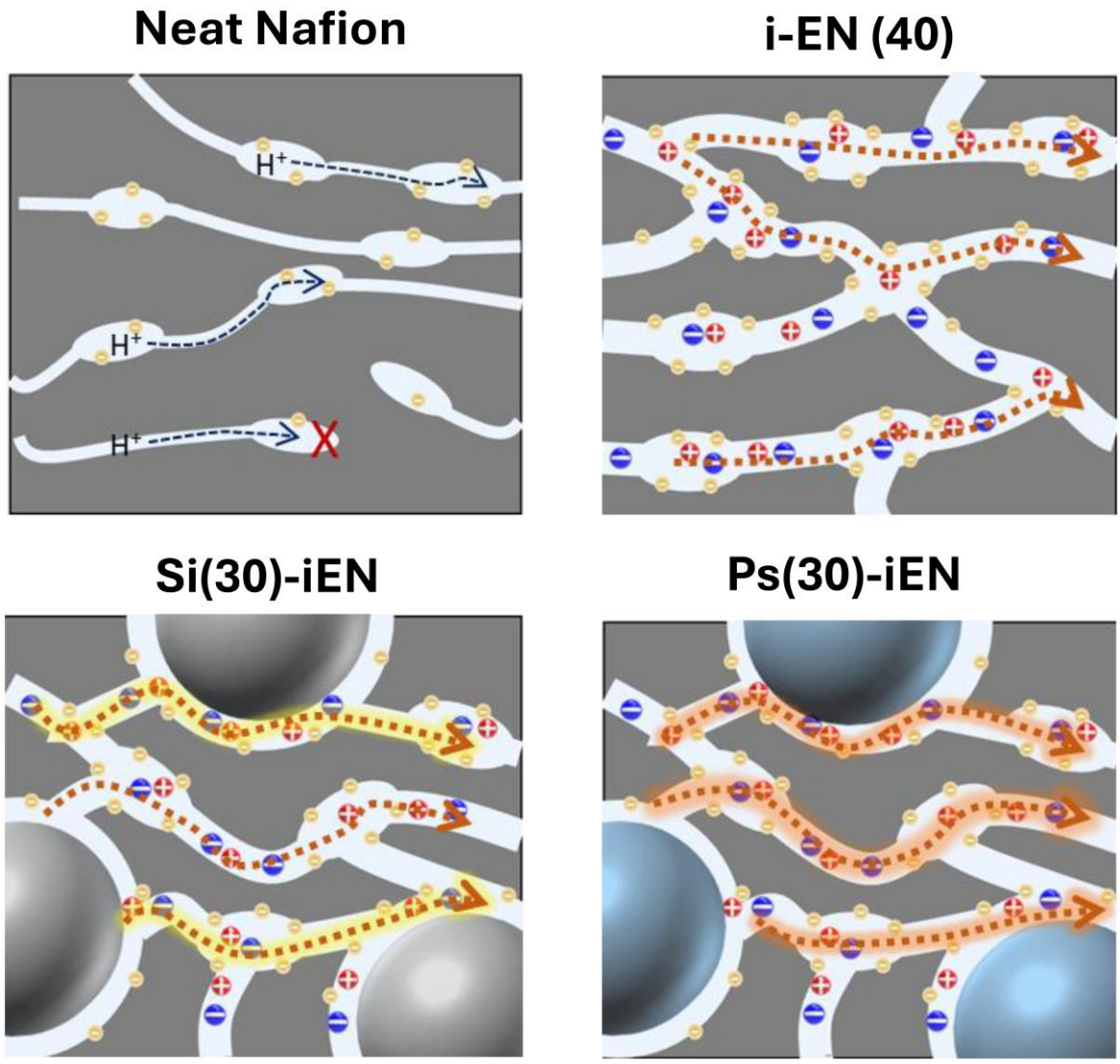

Supplementary Fig. 10. Schematic comparison of ion conduction pathways in Nafion-based electrolytes with varying structural modifications.

(a) Neat Nafion exhibits isolated proton-hopping paths with poor continuity. (b) i-EN(40) with IL incorporation exhibits enhanced ionic cluster formation, but lacks directional ion pathways.
(c) Si(30)-iEN exhibits localized interfacial ion structuring near inorganic fillers, improving pathway connectivity.(d) Ps(30)-iEN exhibits highly aligned and extended conduction pathways mediated by PEG–silica interfaces, enabling more efficient long-range ion transport.

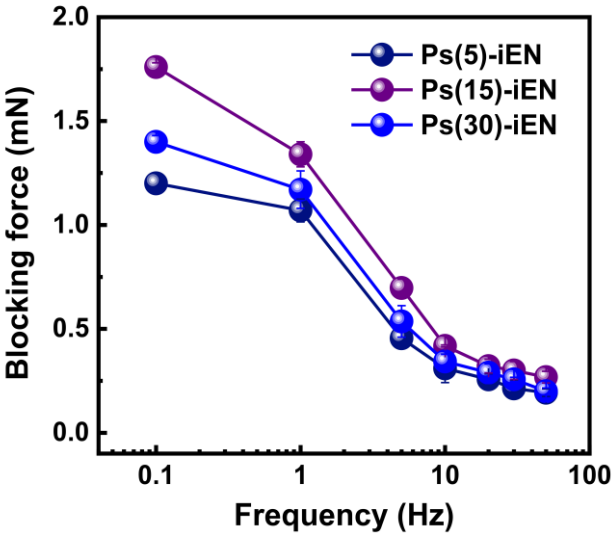

Supplementary Figure 11. Frequency-dependent blocking force curves of Ps(x)-iEN actuators (x = 5, 15, 30) measured at 3 V.

The full blocking-force profiles across 0.1-50 Hz are presented to compare the influence of PEG-silica loading on actuation behavior.

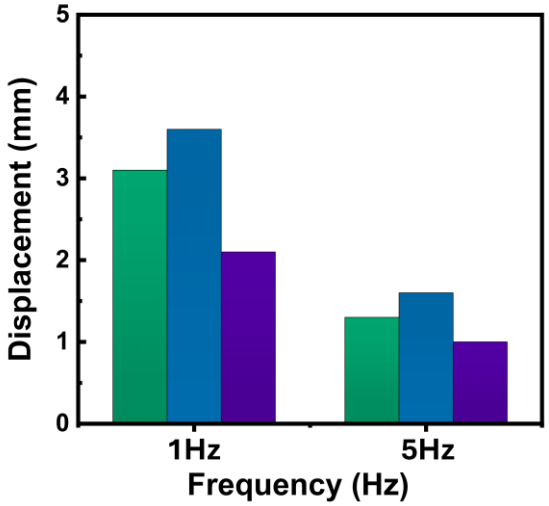

Supplementary Figure 12. Displacement of Ps(x)-iEN actuators at 3 V and two representative frequencies (0.1 and 5 Hz).

Ps(15)-iEN shows the largest displacement, supporting the correlation between σ/E and actuation performance.

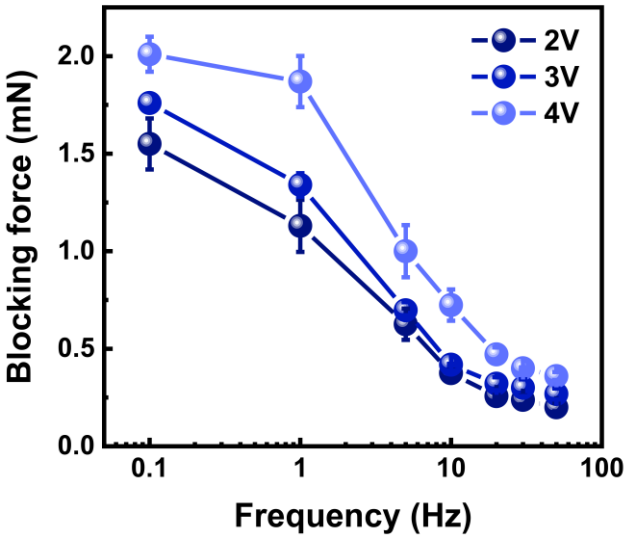

Supplementary Figure 13. Frequency-dependent blocking force curves of the Ps(15)-iEN actuator at different applied voltages (2–4 V).

The complete voltage-frequency response is presented for the optimized composition.

Supplementary Table 1. Comparative summary of the mechanical, ionic conductivity, and design characteristics of representative polymer-based ionic electrolyte systems.

Refer.	Electrolyte	Application	Ionic conductivity (mS/cm)	Modulus (MPa)	Etc.	Year.
[2]	PS-3H4S /Im/HTFSI (2:1)	Actuator	0.8-4.0 (25-80℃)	100	Rod-like ion channels	2022
[18]	Nafion /[EMIM][BF_4]	Actuator	4.5-11	10.4	Continuous conducting network	2024
[24]	Nafion-212 + ZrO_2/Li^+		0.029	66	Formation of salt bridges with $–SO_3H$ groups	2022
[25]	TPU/[EMIM][TFSI] + Silica	Actuator	1.1	5.9	Silica i-TPU Ionic interaction	2023
[26]	PVDF-HFP /[EMIM][BF_4]	Actuator	4.3-7.2 (25-60℃)	22	Continuous conducting network	2022
[27]	Bacterial Cellulose+Mxene/ [EMIM][BF_4]	Actuator	1.46-23.2	33.2	3D interpenetrating BC-MXene frameworks	2023
[28]	BPVA/[EMIM][Cl]	Actuator	0.257	0.11	Bicontinuous phase structure	2023
[29]	PS-3H4S/ [EMIM][TFSI]	Actuator	0.4	3.3	Bifunctional electrolyte (PS-3H4S)	2023
This Study	**Ps-iEN**	**Actuator**	**7.07**	**39**	**PEG-functionalized silica particles**	**2025**

Supplementary Table 2. Comparative summary of representative ionic actuators based on Nafion composite electrolytes, including their composition, mechanical properties, and actuation performance.

Refer.	Electrolyte	Electrode	Ionic conductivity (mS/cm)	Modulus (MPa)	Strain	Force (mN)	Driving Voltage(V)	Operating frequency (Hz)	Year.
[13]	MCNT + Nafion/Li^+	Pt		858.1	33.5mm (@5.0V)	19.2 (@5.0V, DC)	4.2-6.2	0.05-5.0	2022
[16]	Nafion /[EMIM][BF_4]	Porous Carbonaceous Sphere 12 /PEDOT:PSS		52.25	25.5mm (@1.0V)	47.5 (@1.0V, DC)	0.1-1.0	0.1-10	2024
[29]	Nafion /[EMIM][BF_4]	Polysulfonated COF /PEDOT:PSS			0.83% (@1.0V) 9.6mm (@0.5V)	4.76 (@2.0V, DC)	0.01-2.0	0.1-5.0	2023
[41]	Nafion/Cu^+	Pt			10.5 (@3.5V)	10.5 (@3.5V 0.1Hz)	1.5 - 3.5	0.1	2021
[42]	Nafion /HSO_3-SiO_2 /Li^+	Pt			14.54 (@3V)	57.23 (@3V)	2.0-3.0	0.1	2024
[43]	Porous Nafion /[EMIM][SCN]	Pt	0.72		0.666% (@5.0V)	18.36 (@5.0V, 0.1Hz)	3.0-5.0	0.1-10	2020
[44]	Nafion/Li^+	Pt	449		9.46 (@3V)	11.54 (@3V)	1.5–3.5	0.2	2024
[S1]	Nafion /EG/Li^+	Pt			28mm (@3.0V)	38.8 (@4.0V, DC)	2.0-4.0	0.1-10	2023
[S2]	Nafion /[EMIM][BF_4]	MXene / CNT@Fe_3O_4 (MCFe)			12mm (@4.0V)	5.1 (@4.0V, DC)	0.5-4.0	0.1-10	2024
[S3]	Nafion /[EMIM][BF_4]	PEDOT:PSS /DCB-TF	4.7		24mm (@0.5V)	23 (@1.5V, DC)	0.1-1.5	0.01-20	2024
This Study	**Ps-iEN**	**PEDOT:PSS +AgNWS**	**7.07**	**39**	**3.6mm (@3V)**	**2.01 (@4V, 0.1Hz) 0.42 (@4V, 10Hz) 0.36 (@4V, 50Hz)**	**2.0-4.0**	**0.1-60**	**2025**

Supplementary Reference

[1] Liu, C. et al. High water content electrically driven artificial muscles with large and stable deformation for soft robots. *Chem. Eng. J*. **472**, 144700 (2023).

[2] Wu, Ze, et al. Magnetic modulation to construct MXene/CNT@ Fe_3O_4 electrodes with 3D conductive structures for ionic artificial muscles. *Carbon* **221**, 118953 (2024).

[3] Garai, M. et al. Multifunctional and electronically conjugated triazine framework for superior electro-ionic artificial muscles. *Adv. Funct. Mater.* **34**, 2406603 (2024).